

## NGC 770: A Counter-Rotating Core in a Low-Luminosity Elliptical Galaxy

M. Geha<sup>1</sup>

*The Observatories of the Carnegie Institute of Washington, 813 Santa Barbara Street, Pasadena,  
CA 91101*

mgeha@ociw.edu

P. Guhathakurta

*UCO/Lick Observatory, University of California, Santa Cruz, 1156 High Street, Santa Cruz,  
CA 95064*

raja@ucolick.org

and

R. P. van der Marel

*Space Telescope Science Institute, 3700 San Martin Drive, Baltimore, MD 21218*

marel@stsci.edu

### ABSTRACT

We present evidence for a counter-rotating core in the low-luminosity ( $M_B = -18.2$ ) elliptical galaxy NGC 770 based on internal stellar kinematic data. This counter-rotating core is unusual as NGC 770 is not the primary galaxy in the region and it lies in an environment with evidence of on-going tidal interactions. We discovered the counter-rotating core via single-slit Keck\*/ESI echelle spectroscopy; subsequent integral field spectroscopy was obtained with the Gemini/GMOS IFU. The counter-rotating region has a peak rotation velocity of  $21 \text{ km s}^{-1}$  as compared to the main galaxy's rotation speed of greater than  $45 \text{ km s}^{-1}$  in the opposite direction. The counter-rotating region extends to a radius of  $\sim 4''$  (0.6 kpc), slightly smaller than the half-light radius of the

---

<sup>1</sup>Hubble Fellow

\*Data presented herein were obtained at the W. M. Keck Observatory, which is operated as a scientific partnership among the California Institute of Technology, the University of California and the National Aeronautics and Space Administration. The Observatory was made possible by the generous financial support of the W. M. Keck Foundation.

galaxy which is  $5.3''$  (0.8 kpc). The photometry and two-dimensional kinematics suggest that the counter-rotating component is confined to a disk whose scale height is less than  $0.8''$  (0.1 kpc). The major-axis of counter-rotation is misaligned with that of the outer galaxy isophotes by  $15^\circ$ . We compute an age and metallicity of the inner counter-rotating region of  $3 \pm 0.5$  Gyr and  $[\text{Fe}/\text{H}] = 0.2 \pm 0.2$  dex, based on Lick absorption-line indices. The lack of other large galaxies in this region limits possible scenarios for the formation of the counter-rotating core. We discuss several scenarios and favor one in which NGC 770 accreted a small gas-rich dwarf galaxy during a very minor merging event. If this scenario is correct, it represents one of the few known examples of merging between two dwarf-sized galaxies.

*Subject headings:* galaxies: dwarf — galaxies: kinematics and dynamics — galaxies: abundances

## 1. Introduction

Kinematically-distinct cores (KDCs) occur in  $\sim 10\%$  of elliptical galaxies; a few tens of such systems are currently known (Surma & Bender 1995; Mehlert et al. 1998; Wernli et al. 2002; de Zeeuw et al. 2002; De Rijcke et al. 2004; Emsellem et al. 2004). The kinematically-distinct regions have sizes ranging in radius from 0.06 to 2 kpc and have been observed in galaxies which reside in environments ranging from loose groups to dense galaxy clusters. Counter-rotating cores are a subset of KDCs and provide the strongest evidence that these regions are formed during merging events. Balcells & Quinn (1990) investigated the formation of counter-rotating cores via the dissipationless merging of unequal mass elliptical galaxies. In this scenario, the dense core of the smaller galaxy survives the merger and sinks to the center of the primary galaxy via dynamical friction. For certain merging geometries, the surviving core will be kinematically misaligned and will occasionally counter-rotate with respect to its host galaxy. Merging/interactions are not necessarily required to explain kinematically-distinct cores in all cases. Statler (1991) demonstrated that projection effects in a dynamically-smooth triaxial system were able to explain a KDC in NGC 5982 which rotates about its minor-axis. Projection effects, however, do not easily explain cores with counter-rotation about the major axis.

The theories described above cannot naturally explain the presence of faint stellar disks detected on the same scale as the KDCs in several galaxies. In these cases, the more likely formation scenario is the merging or interaction of two separate systems with available gas reservoirs. During the interaction, a disk is formed via the dissipative infall of gas, which eventually cools to form stars (Hernquist & Barnes 1991). Carollo et al. (1997) presented photometric evidence for underlying disks in roughly half of the 15 elliptical galaxies with kinematically-distinct cores they imaged with *Hubble Space Telescope* Wide Field Planetary Camera 2. These authors find no significant color difference between the disk and main galaxy body, although evidence of color differences and

stellar population gradients has been presented in other systems. Mehlert et al. (1998) and Surma & Bender (1995) find evidence for line-strength gradients in three separate systems in the sense that the kinematically-distinct cores have enhanced  $\alpha$ -element to iron abundance ratios relative to the main galaxy, but similarly old ages. They interpret these gradients as evidence of rapid star formation during the formation of the KDC, however, similar gradients have been observed in elliptical galaxies which do not host KDCs (Fisher et al. 1996; Mehlert et al. 2003). In addition to the presence of disks, strong line-strength gradients argue further in favor of dissipational merging since dissipationless processes tend to weaken such gradients.

The majority of known KDCs reside in elliptical galaxies brighter than  $M_B < -19$ . De Rijcke et al. (2004) recently presented evidence for KDCs in two dwarf elliptical galaxies ( $M_V \sim -17$ ) found in galaxy-rich groups. The cores of these two dwarf galaxies rotate in the same direction as the main galaxy body, but with a slower rotation speed. These authors propose an alternative formation mechanism to the merging scenario in which KDCs are formed via flyby interactions between the dwarf and a more massive galaxy. Angular momentum is transferred to the outer envelope of the dwarf during these interactions which results in a kinematic decoupling between the outer envelope and inner core. Such a scenario is favored in dense galaxy environments where the probability of dwarf-dwarf galaxy merging is low due to the large relative velocities between galaxies.

NGC 770 is a low-luminosity elliptical ( $M_B = -18.2$ ) companion to the large spiral galaxy NGC 772, and is the brightest satellite galaxy identified in this system by Zaritsky et al. (1997). The parent spiral galaxy NGC 772 has an absolute magnitude  $M_B = -21.6$  and is listed in the Atlas of Peculiar Galaxies (Arp 78; Arp 1966). This system has been included in many studies of interacting systems (e.g., Pignatelli et al. 2001; Tutui & Sofue 1997; Elmegreen et al. 1991; Laurikainen & Moles 1989) due to a prominent asymmetric spiral arm and faint trails of surrounding material as seen in Figure 1.

Here, we present evidence for a counter-rotating core in the satellite galaxy NGC 770. The counter-rotating core in NGC 770 is particularly interesting as it is one of the faintest elliptical galaxies known to host a counter-rotating core and resides in an environment which shows evidence of recent interactions. This system may provide unique clues to the formation of counter-rotating cores and the presumed role of dissipation in the merging process.

This paper is organized as follows. Observations and reduction procedures for Keck/ESI and Gemini/GMOS IFU data are discussed in §2. We present surface photometry and argue for the presence of a central disk in §3. In §4, we present the one- and two-dimensional kinematic profiles/maps for NGC 770. We measure the stellar absorption-line-strengths in §5 and determine the age and metallicity of the counter-rotating region. In §6, we discuss the environment of NGC 770 and evidence for recent and on-going interactions with the primary galaxy. Finally, in §7, we discuss possible scenarios for the formation of the counter-rotating core in NGC 770.

A true distance modulus to NGC 770 of  $(m-M)_0 = 32.6$ , i.e., a distance of 32.9 Mpc, is adopted

throughout this paper. The distance is determined from the systemic velocity of the primary galaxy in this system, NGC 772, of  $2468 \text{ km s}^{-1}$  (Zaritsky et al. 1997) assuming  $H_0 = 75 \text{ km s}^{-1} \text{ Mpc}^{-1}$ . A line-of-sight extinction value of  $A_V = 0.24$  is adopted from Schlegel, Finkbeiner, & Davis (1998) assuming a standard Galactic reddening law with  $R_V = 3.1$ .

## 2. Observations and Data Reductions

NGC 770 was first confirmed as a satellite galaxy to NGC 772 by Zaritsky et al. (1997) via spectroscopy. The satellite galaxy NGC 770 was targeted for high-resolution spectroscopy as part of our survey of dwarf and low-luminosity elliptical galaxies in a variety of environments (Geha, Guhathakurta, & van der Marel 2003). As seen in Figure 1, NGC 770 lies at a projected distance of only  $3.5'$  (33 kpc) from its parent galaxy. The basic properties of NGC 770 are listed in Table 1.

### 2.1. Single-Slit Keck/ESI Echelle Spectroscopy

Spectroscopic observations of NGC 770 were obtained on 2001 October 12 using the Keck II 10-m telescope and the Echelle Spectrograph and Imager (ESI; Sheinis et al. 2002). The instrument was used in the echellette mode with continuous wavelength coverage over the range  $3900\text{--}11000\text{\AA}$  across 10 echelle orders with a spectral resolution of  $R \equiv \lambda/\Delta\lambda \sim 10,000$ ; our analysis is restricted to the spectral range  $4800\text{--}9200\text{\AA}$  over which useful information can be extracted. The spectra were obtained through a  $0.75'' \times 20''$  slit, resulting in an instrumental resolution of  $23 \text{ km s}^{-1}$  (Gaussian sigma) over the entire spectrum. NGC 770 was observed for  $3 \times 600 \text{ s}$  under seeing conditions of  $0.9''$ . The slit was positioned on the major axis of the galaxy (as determined from Digital Sky Survey images) at a position angle of  $+5^\circ$  on the sky. The ESI data were reduced using a combination of IRAF echelle and long-slit spectral reduction tasks (Geha, Guhathakurta, & van der Marel 2002). The final combined spectrum was rebinned into logarithmic bins with  $11.4 \text{ km s}^{-1}$  per pixel for the kinematic analysis (§ 4.1), and linear bins with  $0.2\text{\AA}$  per pixel for the line-strength analysis (§ 5). In Figure 2, we compare the full spectrum extracted in a  $0.9''$  aperture at the center of the galaxy to a similarly sized aperture  $3''$  off center.

Due to the short ESI slit ( $20''$ ) and the spatial extent of NGC 770, the sky spectrum determined at the extreme edge of the slit contains some galaxy light. We estimate the level of this contamination at  $\sim 2\%$  in the galaxy center, increasing to  $\sim 20\%$  at a radius of  $r = 4''$ . We have tested that galaxy contamination does not affect our results by repeating the analysis using non-local sky subtraction created by combining the sky spectra from unrelated galaxies observed through the same ESI set-up. The resulting kinematic profiles and line-strength values were within the 1-sigma error bars. The results presented in this paper are based on local sky subtraction as this provided the smallest sky-subtraction residuals near bright night-sky lines.

The mean line-of-sight velocity ( $v$ ), velocity dispersion ( $\sigma$ ), and higher-order Gauss-Hermite

moments ( $h_3$  and  $h_4$ ) were determined as a function of radius using a pixel-fitting method described in van der Marel (1994). The velocity profile was recovered using template stars ranging in spectral type from G8 III to M0 III convolved with an appropriate kernel. The best-fitting template, the K0III star HD 6203 ( $[\text{Fe}/\text{H}] = -0.3$  dex), was used to recover the profiles presented here. This stellar template, convolved with the best-fitting Gaussian kernel, is fit to the observed spectra to determine  $v$  and  $\sigma$ ; these parameters are then held fixed while the higher-order deviations from Gaussian are determined. The galaxy data were spatially binned to ensure a minimum signal-to-noise level of  $S/N = 10$  per bin at all radii and a minimum bin-size greater than or equal to that of the seeing FWHM during the observations ( $0.9''$ ). The signal-to-noise ratio in the spatial bins inside  $r = 3''$  is  $S/N \geq 25$ . As demonstrated in Geha et al. (2002), internal velocity dispersions from this observing setup can be measured down to the instrumental resolution of  $23 \text{ km s}^{-1}$  with an accuracy of 1% at our minimum  $S/N$  level. The systemic radial velocity of NGC 770 was determined from the central velocity measurement and subtracted from the velocity profile. The corrected heliocentric systemic velocity is  $v_{\text{sys}} = 2538 \pm 5 \text{ km s}^{-1}$ , in agreement with previous measurements by Zaritsky et al. (1997)  $v_{\text{sys}} = 2543 \pm 22 \text{ km s}^{-1}$ . The one-dimensional Keck/ESI single-slit kinematic profiles are shown in Figure 3.

## 2.2. Gemini/GMOS IFU Spectroscopy

Follow-up two-dimensional spectroscopy of NGC 770 was carried out with the Gemini Multi-object Spectrograph (GMOS; Hook et al. 2004) Integral Field Unit (IFU; Murray et al. 2003) at the Gemini North Telescope on 2003 October 29. The IFU data were obtained in two-slit mode providing a  $5'' \times 7''$  field-of-view consisting of 500  $0.2''$  diameter hexagonal fibers; an additional 250 fibers are dedicated to sky  $1'$  from the science field. We placed the long axis of the IFU along the major axis of the galaxy at a position angle of  $+5^\circ$ . We used the G400 grating and CaT filter which provide wavelength coverage in the region  $7800\text{--}9200\text{\AA}$  with a dispersion of  $0.67\text{\AA}$  per pixel. The spectral resolution is estimated to be  $2.8\text{\AA}$  FWHM, based on the  $0.2''$  fiber diameters, a pixel scale of  $0.072''$  and an anamorphic magnification factor of 0.645. NGC 770 was observed for  $2 \times 3300$  s. The seeing FWHM was  $0.7''$ , estimated from acquisition images taken just prior to the science observations. The data were reduced using the available Gemini IRAF package<sup>2</sup>. The final three-dimensional data cube has  $0.1''$  spatial pixels and  $25 \text{ km s}^{-1}$  spectral pixels.

The mean line-of-sight velocity and velocity dispersion were determined for the GMOS IFU data in the Ca II triplet region ( $8100\text{--}8800\text{\AA}$ ) using the same pixel-fitting method described above (§ 2.1; van der Marel 1994). We determine the optical center of the galaxy from the reconstructed IFU image and set this point equal to  $(x, y) = (0, 0)$  in the kinematic maps. To achieve a minimum signal-to-noise level of  $S/N = 10$  per two-dimensional bin, we spatially rebinned the data using the Voronoi 2D binning algorithm of Cappellari & Copin (2003). A template star taken through

---

<sup>2</sup>Available at <http://gemini.edu/sciops/instruments/gmos/gmosIndex.html>

the same GMOS observing set-up was not available. Instead, velocities were recovered using the same ESI stellar template described in §2.1. The ESI template was rebinned to match the spectral resolution of the GMOS IFU. The measured velocity dispersions are then the quadrature sum of the internal galaxy velocity dispersion and the GMOS instrumental profile. We determine the GMOS instrumental profile by setting the central velocity dispersion equal to that measured in the ESI observations. The instrumental profile is subtracted in quadrature from the measured velocity dispersions to give the internal velocity dispersion of the galaxy. Because it is difficult to determine the shape of the instrumental profile exactly (here we assume it is Gaussian), we do not attempt to recover the higher-order Gauss-Hermite moments for the GMOS IFU data. The resulting mean velocity and velocity dispersion maps for NGC 770 are shown in Figures 4 and 5, respectively.

### 2.3. Keck/ESI Imaging

Keck/ESI  $V$ -band images of NGC 770 were obtained during the same run as the single-slit spectral observations described in §2.1. In imaging mode, ESI has  $0.154''$  pixels and a  $2' \times 8'$  field-of-view. The seeing FWHM was  $0.9''$  in our  $2 \times 60$  s  $V$ -band exposures. The images were bias subtracted, flat fielded using twilight sky exposures, and combined. The photometric zeropoint was determined based on standard star fields taken on a different night from our observations. The resulting image is shown in Figure 6 (left panel). The surface brightness profile was determined using the IRAF ELLIPSE isophotal fitting routine (Jedrzejewski 1987). In Figure 7, radial profiles are shown for surface brightness ( $\mu_V$ ), ellipticity ( $\epsilon$ ), position angle (PA) and higher-order deviations from a perfect ellipse ( $B_4$ ). We fit a Sersic profile to the  $V$ -band surface brightness profile of the form  $I^{\text{gal}}(r) = I_0^{\text{gal}} \exp[(r/r_0)^{1/n}]$ . The best-fit Sersic profile is determined by non-linear least-squares fitting to the region  $r = 1'' - 25''$ ; the best fitting Sersic index for NGC 770 is  $n = 2.3$ . We have also fit a seeing-convolved two-dimensional Sersic profile using the GALFIT fitting algorithm (Peng et al. 2002) in the region  $r < 30''$  and recover the same Sersic index,  $n = 2.3$ . The half-light effective radius, Sersic index, and other photometric quantities agree with previous photometry by Gutiérrez, Azzaro, & Prada (2002) and are listed in Table 1.

## 3. Photometric Analysis

NGC 770 is classified by de Vaucouleurs, de Vaucouleurs, & Corwin (1976) as an “E3:” galaxy, the colon indicating uncertainty in the classification. The source of this uncertainty is due to the shape of the surface brightness profile of this galaxy, shown in Figure 7. The profile is not well fit by either the de Vaucouleurs  $r^{1/4}$  law, nor an exponential profile. Rather, the best fitting Sersic index for NGC 770 is  $n = 2.3$ , intermediate between a  $n = 1$  exponential profile typical for a dwarf elliptical and a  $n = 4$  de Vaucouleurs law typical of giant ellipticals. NGC 770 is half a magnitude brighter ( $M_{V,0} = -18.9$ ) than the brightest classified dwarf elliptical galaxy in the Virgo Cluster and three magnitudes brighter than elliptical satellites NGC 205 and M 32 in the Local Group. It

is best classified as a low-luminosity elliptical galaxy.

Close inspection of the inner photometric contours in Figure 6 (left panel), shows elongated, disk-like central isophotes and boxy isophotes at larger radii. This is quantitatively confirmed by the  $B_4$  profile in Figure 7 which is positive (disky) in the central  $3''$ , and negative (boxy) between radii  $5''$  to  $10''$ . To study the substructure implied by the one-dimensional profile, we plot in Figure 6 (middle panel) the result of subtracting a two-dimensional surface brightness model from the original image. The two-dimensional model is a Sersic  $n = 2.3$  profile at a constant position angle and ellipticity determined at radii  $r \geq 4''$ . In the right panel of Figure 6, we present an unsharp-masked image created by subtracting a boxcar-smoothed image (with a 25 pixel =  $4''$  smoothing length) from the original. Both the model-subtracted and unsharp-masked images suggest a disk in the central region of NGC 770 whose major axis is slightly misaligned with the major axis of the galaxy at larger radii. The central disk extends out to a radius of  $3''$ – $4''$  (0.5–0.6 kpc), slightly less than the half-light radius of the galaxy ( $r_{\text{eff}} = 5.3''$ ). While the vertical extent of this disk is unresolved in the images ( $0.9''$  seeing FWHM), we can put an upper limit on this quantity of  $1''$ . The major axis of the disk-like region seen in the model-subtracted and unsharp-masked image is misaligned by  $15^\circ$  with respect to the major axis of the main galaxy body, consistent with the isophotal twist between the inner and outer regions seen in the position angle profile in Figure 7. To estimate the fraction of light contained in the disk-like region, we compare the flux in the model-subtracted image to that of the original. The model was scaled such that no negative flux was present in the inner  $10''$  of the model-subtracted image. The model-subtracted image contains 6% of the total galaxy light; isolating the elongated disk region inside a radius of  $4''$  represents 3.5% of the total galaxy light. We show below that the inner disk-like region is co-spatial and aligned with the counter-rotating core.

## 4. Stellar Kinematics

### 4.1. One-Dimensional Kinematics

The counter-rotating core in NGC 770 is clearly seen in the major axis Keck/ESI velocity profile shown in the top panel of Figure 3. The mean line-of-sight velocity profile reveals a kinematically-distinct core rotating in a direction opposite to that of the main galaxy body. In these data, the counter-rotating region has an average maximum rotation velocity of  $v_{\text{rot}}^{\text{core}} = 24 \text{ km s}^{-1}$ , but is asymmetric with respect to the galaxy center. We show in §4.2 that this asymmetry is due to a  $\sim 15^\circ$  misalignment of the ESI slit with respect to the major-axis of counter-rotation. The maximum rotation velocity of the main galaxy body is larger than that of the counter-rotating region. We do not reach large enough radius to observe a conclusive turnover in the main galaxy rotation curve and measure a lower limit to the main body rotation of  $v_{\text{rot}}^{\text{gal}} \geq 45 \text{ km s}^{-1}$ . The velocity dispersion profile in Figure 3 is symmetric with respect to the galaxy center, peaking at  $\sigma \sim 100 \text{ km s}^{-1}$  at  $r = \pm 3.5''$  and declining gently in the central regions to a central value of  $76 \text{ km s}^{-1}$ . This central drop in the velocity dispersion profile is observed in other counter-rotating core galaxies

(e.g., Falcón-Barroso et al. 2004) and is usually interpreted as the central region being disk-like and kinematically colder than the outer regions. However, this is not the only interpretation as galaxies without counter-rotating cores often show similar drops in the central velocity dispersion (Magorrian et al. 1998; Geha et al. 2003).

If the main body of NGC 770 were supported by rotational motion then the expected ratio of the maximum rotation velocity to central velocity dispersion would be  $v_{\text{rot}}/\sigma = 0.7$  given a measured ellipticity of  $\epsilon = 0.33$  (Binney & Tremaine 1987). The observed ratio is  $v_{\text{rot}}/\sigma = 0.47$ , but is a lower limit due to our limited radial coverage. It is likely that the main galaxy body of NGC 770 is rotationally supported, consistent with what is seen in elliptical galaxies of similar luminosity (Davies et al. 1983).

The bottom two panels of Figure 3 show the radial profiles of the Gauss-Hermite moments  $h_3$  and  $h_4$ . These parameters measure the deviations of the line-of-sight velocity profile from a Gaussian profile. The  $h_3$  parameter measures asymmetric deviations, while  $h_4$  measures symmetric deviations. The  $h_3$  profile in Figure 3 has the same shape as the velocity profile, but with opposite sign. The  $h_4$  parameter peaks at negative values (a flatter than Gaussian velocity profile) where the counter-rotating velocity returns to zero. A plausible interpretation of the  $h_3$  profile is the presence of two kinematically-distinct components: in the counter-rotating region, the lower velocity stars of the main galaxy produce an asymmetric tail in the velocity profile in a direction opposite that of rotation. However, this sign difference between the  $h_3$  and velocity profiles is also seen in galaxies without counter-rotating cores (eg. Emsellem et al. 2004). Thus, although the higher-order moments suggest the presence of two kinematic components in the inner region of NGC 770, it is hard to provide an unambiguous interpretation of these data.

## 4.2. Two-Dimensional Kinematics

The two-dimensional Gemini/GMOS IFU velocity (Figure 4) and velocity dispersion (Figure 5) maps confirm the counter-rotating core in NGC 770 and provide evidence that stars in this region are moving in a disk. The velocity of the counter-rotating core is symmetric with respect to the photometric center of the galaxy, peaking at a maximum velocity of  $v_{\text{rot}}^{\text{core}} = \pm 21 \text{ km s}^{-1}$  at a spatial position of  $(x, y) = (0.97'', 0.13'')$  and  $(-0.95'', -0.2'')$  in Figure 4. In the top panel of this figure, we show a one-dimensional velocity profile determined by averaging over a  $0.75''$  wide slit placed along the major axis of counter-rotation. Unlike the single-slit Keck/ESI data shown in Figure 3, the velocity profile is symmetric, peaking at a radial distance of  $r = \pm 1''$ . The velocity dispersion map in Figure 5 shows a colder, lower velocity dispersion central region which is slightly elongated along the axis of counter-rotation.

We estimate the size of the counter-rotating region by fitting an ellipse to a zero-velocity contour in Figure 4 excluding the central half arcsecond. The best fitting ellipse has a semi-major axis of  $3.5''$  and semi-minor axis of  $0.8''$ . The seeing during these observations was  $0.7''$  FWHM.



Thus, we are able to put an upper limit on the scale height of the counter-rotating disk of  $0.8'' = 130$  pc due to both seeing limitations and the unknown inclination angle. This is consistent with the photometric estimates of the disk size presented in § 3.

The position angle of the best-fitting zero-velocity ellipse in Figure 4 is  $15^\circ$  relative to the major-axis of the main galaxy or  $20^\circ$  East of North. This misalignment between the main galaxy body and the counter-rotating core is consistent with the isophotal twist measured between the inner and outer galaxy in § 3. This misalignment is sufficient to explain the asymmetry observed in the single-slit ESI velocity profile which was placed along the photometric major axis of the main galaxy body.

## 5. Line-Strength Index Profiles

We compute line-strength indices according to the Lick/IDS system (Worthey et al. 1994) in the wavelength region  $4800 - 6000\text{\AA}$ . Lick indices are calculated only for the one-dimensional ESI spectra since the two-dimensional GMOS IFU data are confined to a narrow spectral region. A more detailed description of the procedures to measure line-strength indices for ESI data is provided in Geha et al. (2003). Briefly, line-strength indices were computed by shifting the ESI spectra to rest frame wavelengths and convolving with a wavelength-dependent Gaussian kernel to match the spectral resolution of the Lick/IDS system. The size of the kernel ranged between  $8 - 9\text{\AA}$  ( $40 - 45$  ESI spectral pixels, Gaussian sigma). Line-strengths were then calculated according to the index definitions of Worthey et al. (1994). Error bars on the indices were computed via Monte-Carlo simulations which include contributions from photon noise, read-out noise and pixel-to-pixel correlations due to Gaussian smoothing.

We compare the weighted average line-strengths for the inner ( $r \leq 2''$ ) and outer ( $2'' < r < 4''$ ) counter-rotating core plotted as solid and open points, respectively, in Figure 8. We do not measure line-strengths beyond the counter-rotating region ( $r > 4''$ ) due to insufficient signal-to-noise. However, because the ESI slit was slightly misaligned with respect to the counter-rotating disk, the outer measurement will contain more light from the main galaxy as compared to the inner measurement. To determine the luminosity-weighted stellar ages and metallicities, we plot the Mg b and  $\langle \text{Fe} \rangle$  (where  $\langle \text{Fe} \rangle \equiv (\text{Fe}5270 + \text{Fe}5335)/2$ ) indices against  $\text{H}\beta$  in Figure 8. We compare our line-strength indices to the single-burst solar metallicity stellar population models of Thomas, Maraston, & Bender (2003). The best fitting ages and metallicities were determined by simultaneously minimizing the residuals between the observed line-strengths and the predicted Mg b,  $\langle \text{Fe} \rangle$ , and  $\text{H}\beta$  indices from the Thomas et al. solar abundance models. The best fitting age and metallicity for the inner counter-rotating region is  $3 \pm 0.5$  Gyr and  $[\text{Fe}/\text{H}] = 0.2 \pm 0.2$  dex, and for the outer core region  $8 \pm 2$  Gyr and  $[\text{Fe}/\text{H}] = -0.1 \pm 0.2$ . Although the absolute ages and metallicities are subject to systematic errors in the models, the *relative* ages between the two components are more secure.

The difference between the line-strengths measured in the inner and outer core may be due to a stellar population gradient within the counter-rotating region or represent contamination from the main galaxy in the outer measurement. We favor the latter interpretation since the age and metallicity for the outer core agree with the global line-strength measurements presented by Caldwell et al. (2003) of NGC 770. The outer core is consistent with the average age and metallicity measured for a sample of dwarf elliptical galaxies of comparable and fainter luminosities presented by Geha et al. (2003). The age of the inner counter-rotating region is younger than for typical dwarf elliptical galaxies. The stronger  $H\beta$  index in the inner core compared to the outer region suggests that the counter-rotating component contains a younger stellar population relative to the main galaxy body.

## 6. The Environment of NGC 770

NGC 770 is a low-luminosity elliptical galaxy companion to the large spiral galaxy NGC 772. The parent galaxy NGC 772 has an absolute magnitude  $M_B = -21.6$  and is isolated, having no neighbors brighter than  $M_B \leq -19$  within  $1000 \text{ km s}^{-1}$  and  $1.75^\circ$  (1 Mpc) in the NASA/IPAC Extragalactic Database<sup>3</sup>. In addition to NGC 770, Zaritsky et al. (1997) identified two other fainter ( $M_B \sim -16$ ) satellites in this system at projected distances  $\sim 400$  kpc. Additional fainter satellite galaxies are likely present in this system. NGC 770 is the closest and brightest satellite galaxy to NGC 772 with an absolute magnitude of  $M_B = -18.2$  and a projected distance of  $r_p = 3.5' = 32$  kpc. The physical separation of NGC 770 to its parent galaxy is larger than that of the Milky Way and the Sagittarius dwarf galaxy (24 kpc; Ibata et al. 1995), and is likely comparable to that of the Large Magellanic Cloud (50 kpc; Freedman et al. 2001) or NGC 205 and M31 (van den Bergh 2000).

The primary spiral galaxy, NGC 772, is listed in the Atlas of Peculiar Galaxies (Arp 78; Arp 1966) due to a prominent asymmetric spiral arm and faint trails of material surrounding both the primary spiral and the satellite elliptical NGC 770 (Figure 1). Pignatelli et al. (2001) showed that the inner 10 kpc of this spiral are symmetric, and successfully model the inner spiral region assuming dynamic equilibrium. The asymmetric region outside 10 kpc is due to a single prominent spiral arm which is also the primary region of on-going star formation; the majority of the  $H\alpha$  flux in this galaxy is emitted in this region (Laurikainen & Moles 1989).

---

<sup>3</sup>This research has made use of the NASA/IPAC Extragalactic Database (NED) which is operated by the Jet Propulsion Laboratory, California Institute of Technology, under contract with the National Aeronautics and Space Administration.

### 6.1. The Distribution of HI Gas in the NGC 772/770 System

The neutral hydrogen (HI) gas in the NGC 772/770 system extends well beyond the optical radius of NGC 772 and is highly disturbed. This system was observed in the 21 cm line by Iyer et al. (2001) with the Very Large Array (VLA) in the D-configuration. The observing set-up and reduction procedures are similar to those discussed in Iyer et al. (2004). The HI flux density map shown in the left panel of Figure 9 was first presented as a minor merger system in the HI Rogues Gallery (Hibbard et al. 2001). The corresponding HI velocity map in the right panel of this figure was kindly provided to us by C. Simpson. The total HI mass in this system is  $2.6 \times 10^{10} M_{\odot}$  (Broeils & Rhee 1997).

The integrated HI distribution in the NGC 772/770 system is not centered on the primary galaxy, instead it is skewed toward the satellite galaxy NGC 770 and extends well beyond the projected distance of the satellite. The HI velocity map in the right panel of Figure 9 shows regular rotation in the inner region of the primary galaxy and a velocity gradient along the outer arm of material. A deficiency in the HI distribution is seen in the region of NGC 770. Although HI has been detected in NGC 770 (Huchtmeier & Richter 1989), the integrated flux density is below the detection threshold of the VLA observations. This deficiency can be interpreted as either a hole in the HI distribution, or the inner region of an HI arm which has wrapped around the primary galaxy. The asymmetry of the HI distribution requires a recent interaction, we discuss possible scenarios below.

## 7. The Influence of Interactions on NGC 770 and its Counter-Rotating Core

The discovery of a counter-rotating core in NGC 770 is unusual as this host is not the primary galaxy in this system and it lies in a region of on-going tidal interactions. Ongoing star formation in the asymmetric arm of the primary galaxy NGC 772, and the short dynamical lifetime of such a structure requires a triggering interaction in the past few 100 Myrs (Elmegreen et al. 1991; Pignatelli et al. 2001). The NGC 772/770 system is isolated—the lack of any other massive objects in this system strongly suggests that this most recent interaction involved NGC 772 and NGC 770. The presence of a faint optical trail of material close to satellite galaxy NGC 770 (Figure 1) and its position relative to the HI gas distribution (Figure 9) support this hypothesis. The mass ratio between these two galaxies is 20:1, assuming they have similar mass-to-light ratios. Careful modeling is required to understand the details of this interaction.

Although it is likely that NGC 772 and NGC 770 are undergoing (or have recently undergone) tidal interaction, the counter-rotating core in NGC 770 could not have been formed during these most recent interactions. The inferred age of the counter-rotating core in the satellite galaxy NGC 770 is 3 Gyr, longer than a reasonable estimate for the orbital period of NGC 770. The radial velocity difference between between NGC 772 and NGC 770 is  $70 \text{ km s}^{-1}$ . Assuming a transverse velocity comparable to the measured radial velocity, the space velocity of NGC 770 is

$\sqrt{3} \times 70 \sim 120 \text{ km s}^{-1}$ . If the projected distance of NGC 770 is the radius of its orbit around NGC 772, then its orbital period is 1.5 Gyr. If NGC 770 is currently on an unbound orbit, it would have been roughly 500 kpc from NGC 772 at the time of the counter-rotating core’s formation. Thus, the counter-rotating core in NGC 770 was formed somewhere between the outskirts of this group or closer to the primary galaxy NGC 772, two to three orbits ago.

The lack of other large galaxies in this region limit the possible formation scenarios for the formation of the counter-rotating core in NGC 770. We discuss several possibilities: (1) NGC 770 accreted a small dwarf galaxy during a very minor merging event, (2) NGC 770 accreted material from the primary galaxy during earlier orbital interactions, or (3) the counter-rotating region was formed via angular momentum transfer to the outer envelope of the galaxy via harassment. The age difference between the core and the main body of NGC 770 (§5) suggest that the counter-rotating region was not formed concurrently with the main galaxy. The absolute age of the counter-rotating region of 3 Gyr suggests that it was not formed during the interactions which caused the disturbances seen in the primary spiral galaxy NGC 772 since these features have dynamical lifetimes of 100 Myr. Observational evidence presented in §3 and §4.2 suggests that the counter-rotating stars in NGC 770 are moving in a disk. Thus, any plausible formation mechanism must explain the counter-rotation, the age difference between the core and main galaxy body as well as the presence of a central disk.

A minor merging event which did not destroy NGC 770 but did provide material with very different angular momentum can explain the observed counter-rotating core in this galaxy. Evidence that the counter-rotating stars rotate in a disk suggests that the merged galaxy contained a significant gas fraction. If the core was formed in such a scenario, the galaxy which merged with NGC 770 would necessarily be a small dwarf galaxy. In §3, we estimate that the inner disk region of NGC 770 contains  $\sim 3.5\%$  of the total galaxy light. If we attribute this to the counter-rotating component, it corresponds to an absolute luminosity of  $M_V \sim -15$  or a mass of  $\sim 10^8 M_\odot$  modulo the unknown gas fraction in such a progenitor and the efficiency of star formation in low-mass mergers.

The abundance of HI gas in the NGC 772/770 system makes it possible that the counter-rotating core formed via gas accretion from the primary galaxy. It appears from Figure 9 that NGC 770 is affecting the HI gas distribution of NGC 772. However, these current interactions have a dynamical timescale that is much shorter than the inferred age of the counter-rotating disk. Thus, this gas accretion would have had to have occurred two to three orbits ago in NGC 770’s motion around its primary galaxy. Although it may be possible, it is unlikely that gas from the primary galaxy would be accreted by the smaller perturbing galaxy far from the center of mass of the system.

NGC 770 is the faintest known galaxy to host a core which counter-rotates with respect to the main galaxy kinematics. De Rijcke et al. (2004) propose an alternative formation mechanism for kinematically-distinct cores in low luminosity ellipticals in which angular momentum is transferred

to the halo of a dwarf galaxy during flyby encounters with more massive galaxies. These authors present observations of two dwarf elliptical galaxies ( $M_B \sim -17$ ) with cores rotating in the same direction as the main galaxy body, but with slower rotation speeds. In these two systems, the kinematic decoupling observed between the core and halo can be explained via galaxy interactions. In the case of NGC 770, the maximum angular momentum transfer during its current encounter between NGC 770 and its parent galaxy is  $\sim 2 \text{ km s}^{-1}$  (assuming a relative velocity of  $120 \text{ km s}^{-1}$ , separation distance of 32 kpc, and primary galaxy mass  $2 \times 10^{11} M_\odot$ ; c.f. Eqn. 7 of De Rijcke et al. (2004)). To explain the counter-rotating core in NGC 770, which rotates with a maximum velocity of  $21 \text{ km s}^{-1}$  in a direction opposite the main galaxy, would require either an unreasonably large number of orbits at the current separation, or fewer orbits at a closer physical separation. Thus, interactions are an unlikely formation mechanism for the counter-rotating core in NGC 770.

Of the above formation models, we favor the scenario in which the counter-rotating core in NGC 770 was formed during a minor merging event with a smaller dwarf galaxy. De Rijcke et al. (2004) have noted that dwarf-dwarf merging is unlikely in galaxy-rich groups and clusters due to large relative velocities between galaxies. In the low galaxy density environment of NGC 770, the low relative velocities ( $\sim 100 \text{ km s}^{-1}$ ) suggests that NGC 770 could have captured a smaller dwarf galaxy for impact parameters less than a few tens of kpc. If the merging scenario is correct, NGC 770 is an excellent example of merging at dwarf-sized galaxy scales.

## 8. Summary

We present evidence for a counter-rotating core in the low-luminosity elliptical galaxy NGC 770 based on Keck/ESI and Gemini/GMOS IFU spectroscopy. The combined one- and two-dimensional kinematics argue for a kinematically-distinct core rotating counter to the main galaxy body with maximum rotation speed of  $21 \text{ km s}^{-1}$ . The counter-rotating region is misaligned with the main body of the galaxy by  $15^\circ$ . We present evidence that stars in the counter-rotating region are confined to a disk with radius  $4''$  (0.6 kpc) and we estimate an upper limit to the scale disk height of  $0.8''$  (0.1 kpc). We compute an age and metallicity of the inner counter-rotating region of  $3 \pm 0.5 \text{ Gyr}$  and  $[\text{Fe}/\text{H}] = 0.2 \pm 0.2 \text{ dex}$ , based on Lick absorption-line indices. We discuss several possible formation scenarios for the counter-rotating core in NGC 770 and favor one in which the core was formed in a minor merging event with a smaller dwarf galaxy. If this scenario is correct, it represents one of the few known examples of merging between two dwarf-sized galaxies.

We are grateful to M. Iyer and C. Simpson (FIU) for kindly providing the VLA HI map of NGC 772/770 before publication. We thank Jeremy Darling and Francois Schweizer for fruitful discussions regarding this work. M. G. is supported by NASA through Hubble Fellowship grant HF-01159.01-A awarded by the Space Telescope Science Institute, which is operated by the Association of Universities for Research in Astronomy, Inc., under NASA contract NAS 5-26555. P. G. acknowledges support from NSF grant AST-0307966. Based in part on observations obtained

at the Gemini Observatory (Program ID GN-2003B-Q-42), which is operated by the Association of Universities for Research in Astronomy, Inc., under a cooperative agreement with the NSF on behalf of the Gemini partnership: the National Science Foundation (United States), the Particle Physics and Astronomy Research Council (United Kingdom), the National Research Council (Canada), CONICYT (Chile), the Australian Research Council (Australia), CNPq (Brazil) and CONICET (Argentina).

## REFERENCES

- Arp, H. 1966, *ApJS*, 14, 1
- Balcells, M., & Quinn, P. J. 1990, *ApJ*, 361, 381
- Binggeli, B., Sandage, A., & Tammann, G. A. 1985, *AJ*, 90, 1681
- Binney, J., & Tremaine, S. 1987, *Galactic Dynamics* (Princeton, NJ, Princeton University Press, 1987)
- Broeils, A. H., & Rhee, M.-H. 1997, *A&A*, 324, 877
- Caldwell, N., Rose, J. A., & Concannon, K. D. 2003, *AJ*, 125, 2891
- Cappellari, M., & Copin, Y. 2003, *MNRAS*, 342, 345
- Carollo, C. M., Franx, M., Illingworth, G. D., & Forbes, D. A. 1997, *ApJ*, 481, 710
- Davies, R. L., Efstathiou, G., Fall, S. M., Illingworth, G., & Schechter, P. L. 1983, *ApJ*, 266, 41
- De Rijcke, S., Dejonghe, H., Zeilinger, W. W., & Hau, G. K. T. 2004, *astro-ph/0407425*
- de Vaucouleurs, G., de Vaucouleurs, A., & Corwin, J. R. 1976, in *Second reference catalogue of bright galaxies, 1976*, Austin: University of Texas Press.
- de Zeeuw, P. T., Bureau, M., Emsellem, E., Bacon, R., Marcella Carollo, C., Copin, Y., Davies, R. L., Kuntschner, H., Miller, B. W., Monnet, G., Peletier, R. F., & Verolme, E. K. 2002, *MNRAS*, 329, 513
- Elmegreen, D. M., Sundin, M., Sundelius, B., & Elmegreen, B. 1991, *A&A*, 244, 52
- Emsellem, E., Cappellari, M., Peletier, R. F., McDermid, R. M., Bacon, R., Bureau, M., Copin, Y., Davies, R. L., Krajnović, D., Kuntschner, H., Miller, B. W., & Tim de Zeeuw, P. 2004, *MNRAS*, 352, 721
- Falcón-Barroso, J., Peletier, R. F., Emsellem, E., Kuntschner, H., Fathi, K., Bureau, M., Bacon, R., Cappellari, M., Copin, Y., Davies, R. L., & de Zeeuw, T. 2004, *MNRAS*, 350, 35

- Fisher, D., Franx, M., & Illingworth, G. 1996, *ApJ*, 459, 110
- Freedman, W. L., Madore, B. F., Gibson, B. K., Ferrarese, L., Kelson, D. D., Sakai, S., Mould, J. R., Kennicutt, R. C., Ford, H. C., Graham, J. A., Huchra, J. P., Hughes, S. M. G., Illingworth, G. D., Macri, L. M., & Stetson, P. B. 2001, *ApJ*, 553, 47
- Geha, M., Guhathakurta, P., & van der Marel, R. P. 2002, *AJ*, 124, 3073
- . 2003, *AJ*, 126, 1794
- Gutiérrez, C. M., Azzaro, M., & Prada, F. 2002, *ApJS*, 141, 61
- Hernquist, L., & Barnes, J. E. 1991, *Nature*, 354, 210
- Hibbard, J. E., van Gorkom, J. H., Rupen, M. P., & Schiminovich, D. 2001, in *ASP Conf. Ser. 240: Gas and Galaxy Evolution*
- Hook, I. M., Jørgensen, I., Allington-Smith, J. R., Davies, R. L., Metcalfe, N., Murowinski, R. G., & Crampton, D. 2004, *PASP*, 116, 425
- Huchtmeier, W. K., & Richter, O.-G. 1989, *A General Catalog of HI Observations of Galaxies. The Reference Catalog. (A General Catalog of HI Observations of Galaxies. The Reference Catalog, XIX, 350 pp. 8 figs.. Springer-Verlag Berlin Heidelberg New York)*
- Ibata, R. A., Gilmore, G., & Irwin, M. J. 1995, *MNRAS*, 277, 781
- Iyer, M. G., Simpson, C. E., Gottesman, S. T., Hargis, J. R., & Malphrus, B. K. 2001, in *ASP Conf. Ser. 240: Gas and Galaxy Evolution*, 861
- Iyer, M. G., Simpson, C. E., Gottesman, S. T., & Malphrus, B. K. 2004, *AJ*, 128, 985
- Jedrzejewski, R. I. 1987, *MNRAS*, 226, 747
- Laurikainen, E., & Moles, M. 1989, *ApJ*, 345, 176
- Magorrian, J., Tremaine, S., Richstone, D., Bender, R., Bower, G., Dressler, A., Faber, S. M., Gebhardt, K., Green, R., Grillmair, C., Kormendy, J., & Lauer, T. 1998, *AJ*, 115, 2285
- Mehlert, D., Saglia, R. P., Bender, R., & Wegner, G. 1998, *A&A*, 332, 33
- Mehlert, D., Thomas, D., Saglia, R. P., Bender, R., & Wegner, G. 2003, *A&A*, 407, 423
- Murray, G. J., Allington-Smith, J. R., Content, R., Davies, R. L., Dodsworth, G. N., Miller, B., Jørgensen, I., Hook, I., Crampton, D., & Murowinski, R. G. 2003, in *Instrument Design and Performance for Optical/Infrared Ground-based Telescopes*. Edited by Iye, Masanori; Moorwood, Alan F. M. *Proceedings of the SPIE, Volume 4841, pp. 1750-1759 (2003).*, 1750–1759

- Peng, C. Y., Ho, L. C., Impey, C. D., & Rix, H. 2002, *AJ*, 124, 266
- Pignatelli, E., Corsini, E. M., Vega Beltrán, J. C., Scarlata, C., Pizzella, A., Funes, J. G., Zeilinger, W. W., Beckman, J. E., & Bertola, F. 2001, *MNRAS*, 323, 188
- Schlegel, D. J., Finkbeiner, D. P., & Davis, M. 1998, *ApJ*, 500, 525
- Sheinis, A. I., Bolte, M., Epps, H. W., Kibrick, R. I., Miller, J. S., Radovan, M. V., Bigelow, B. C., & Sutin, B. M. 2002, *PASP*, 114, 851
- Statler, T. S. 1991, *ApJ*, 382, L11
- Surma, P., & Bender, R. 1995, *A&A*, 298, 405
- Thomas, D., Maraston, C., & Bender, R. 2003, *MNRAS*, 339, 897
- Tutui, Y., & Sofue, Y. 1997, *A&A*, 326, 915
- van den Bergh, S. 2000, *PASP*, 112, 529
- van der Marel, R. P. 1994, *MNRAS*, 270, 271
- Wernli, F., Emsellem, E., & Copin, Y. 2002, *A&A*, 396, 73
- Worthey, G., Faber, S. M., Gonzalez, J. J., & Burstein, D. 1994, *ApJS*, 94, 687
- Zaritsky, D., Smith, R., Frenk, C., & White, S. D. M. 1997, *ApJ*, 478, 39



Table 1. NGC 770: Basic Properties

Name	$\alpha$ (J2000) (h:m:s)	$\delta$ (J2000) ( $^{\circ}$ : $'$ : $''$ )	Type	$m_V$	$A_V$	$M_{V,0}$	$\epsilon$	$r_{\text{eff}}$ [ $''$ (kpc)]	$\mu_{V,\text{eff}}$ (mag arcs $^{-2}$ )	$n_{\text{serc}}$
NGC 770	1:59:13.6	18:57:17	E3:	13.9	0.24	−18.9	0.33	5.2 (0.83)	19.5	2.3

Note. — Galaxy classification taken from Binggeli et al. (1985); the “:” indicates uncertainty in the classification. The apparent magnitude is determined from Keck/ESI  $V$ -band imaging inside an  $r < 40''$  aperture. The absolute magnitude,  $M_{V,0}$ , assumes a distance modulus of  $(m - M)_0 = 32.6$  and is corrected for foreground reddening according to Schlegel et al. (1998).

Table 2. NGC 770: Line-Strength Indices

	H $\beta$ ( $\text{\AA}$ )	Mgb ( $\text{\AA}$ )	$\langle \text{Fe} \rangle$ ( $\text{\AA}$ )
Inner core ( $r < 2''$ )	$2.18 \pm 0.07$	$3.39 \pm 0.04$	$2.58 \pm 0.06$
Outer core ( $2'' < r < 4''$ )	$1.78 \pm 0.11$	$3.32 \pm 0.08$	$2.52 \pm 0.11$

Note. — Line-strength indices are determined according to the definitions of Worthey et al. (1994). Error bars are computed via Monte-Carlo simulations as described in §5. The combined iron index is defined as  $\langle \text{Fe} \rangle \equiv (\text{Fe}5270 + \text{Fe}5335)/2$ .

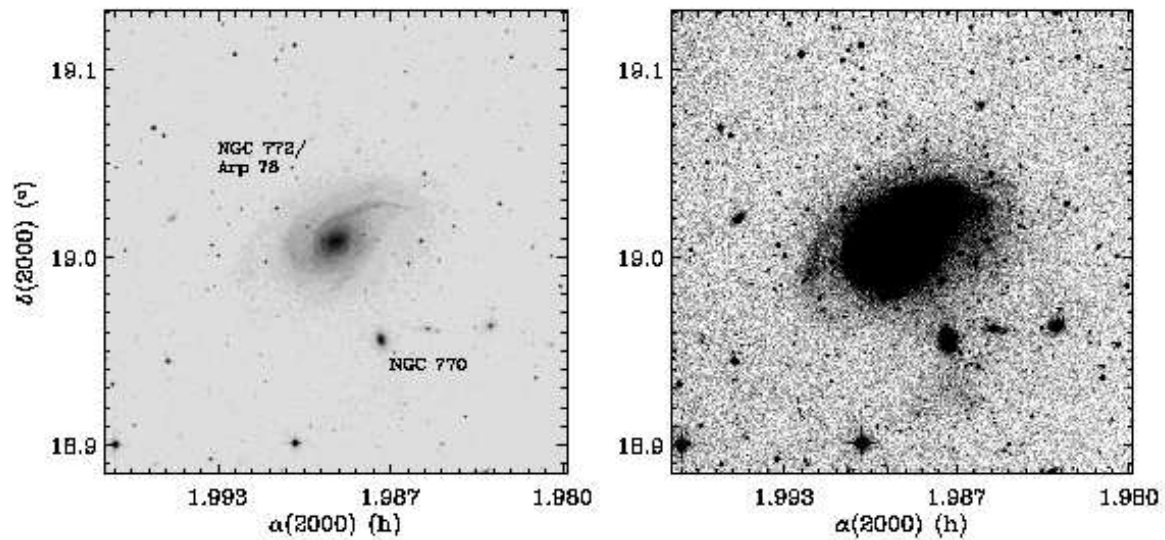


Fig. 1.— The environment of the low-luminosity elliptical galaxy NGC 770. (*Left*) Digitized Palomar Optical Sky Survey-II image centered on the parent spiral galaxy NGC 772/Arp 78; the satellite NGC 770 is located  $4'$  to the SW of the primary spiral. The image is  $15' \times 15'$ . (*Right*) Same image displayed at higher contrast to highlight the faint tidal features extending from both NGC 772 and NGC 770.

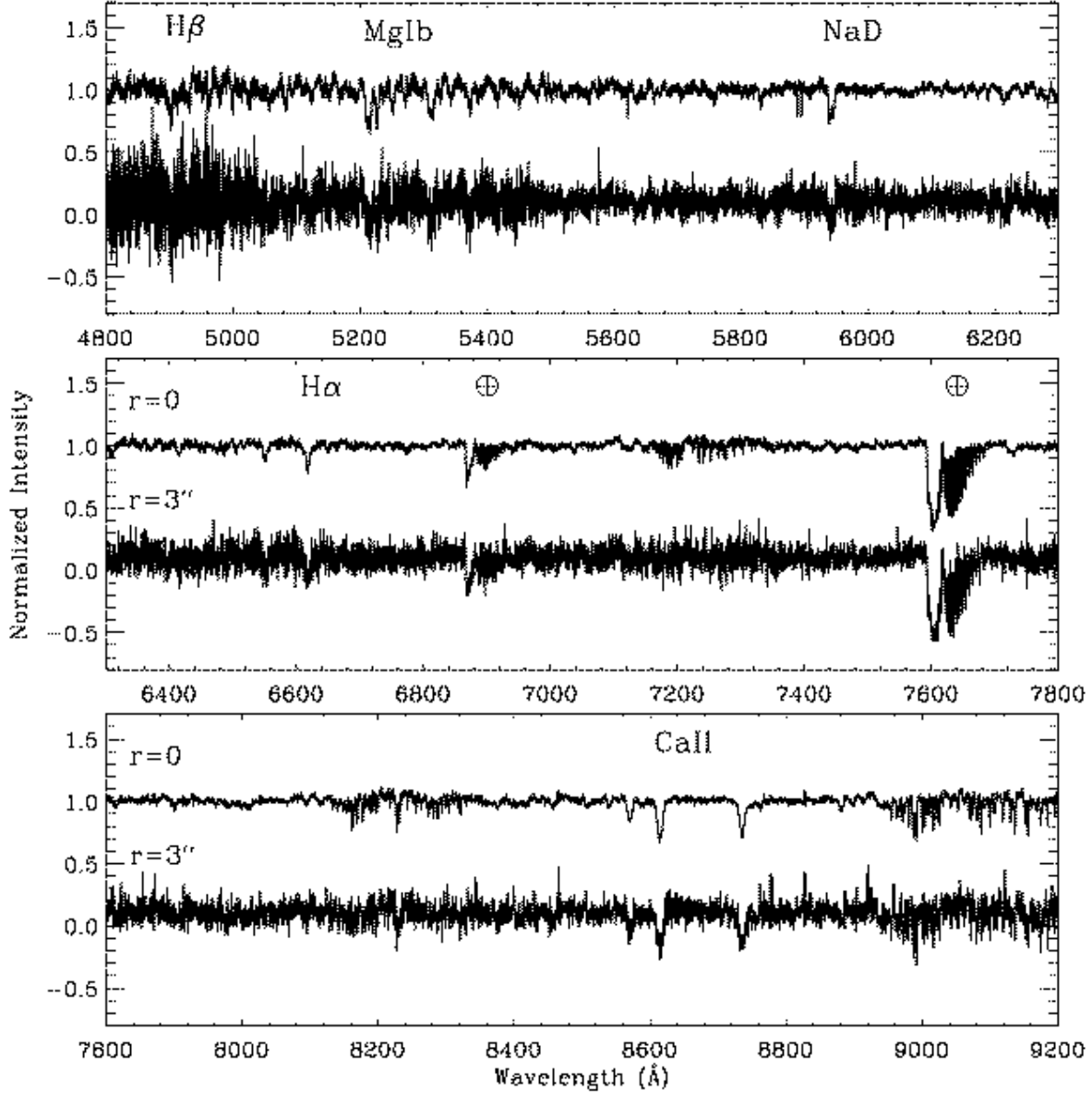


Fig. 2.— Keck/ESI echelle spectra of NGC 770 covering the continuous wavelength region 4800–9200Å. Spectra are shown for the galaxy center ( $r = 0''$ ) and the edge of the counter-rotating region ( $r = 3''$ ). The spectra are binned spatially to  $0.9''$ , the seeing FWHM at the time of the observations, but have not been smoothed in the spectral direction. A few of the important stellar absorption features are indicated, along with the atmospheric A and B absorption bands.

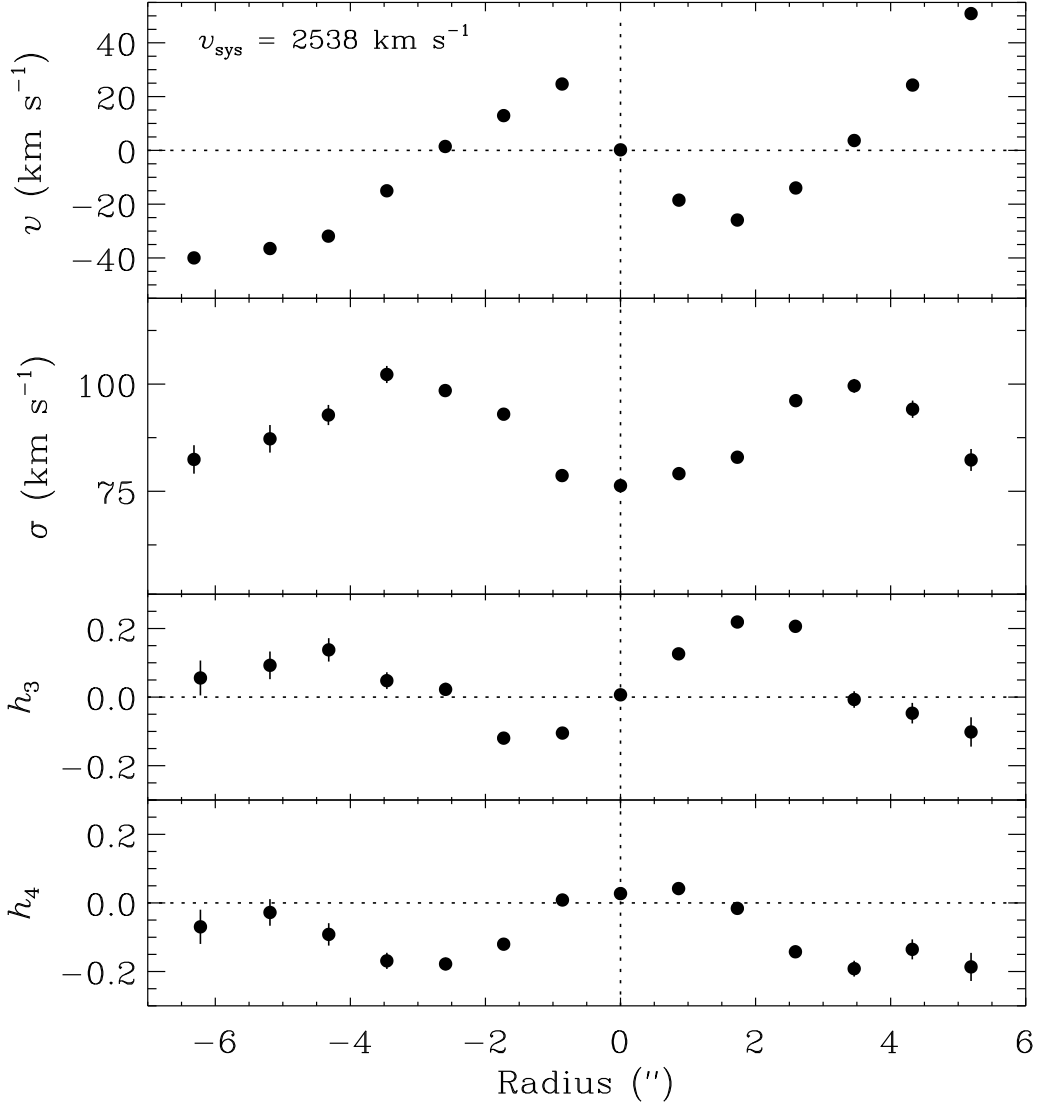


Fig. 3.— (*Top to bottom*) Radial profiles of the mean line-of-sight velocity  $v$ , velocity dispersion  $\sigma$ , and higher-order Gauss-Hermite moments,  $h_3$  and  $h_4$ , measured via Keck/ESI single-slit observations. The slit was placed along the photometric major axis of the main body of NGC 770, which is misaligned with respect to the kinematic major axis of the counter-rotating region by  $15^\circ$ . The velocity profile reveals a kinematically-distinct core rotating in a direction opposite to that of the main galaxy body. At the distance of NGC 770,  $1'' = 160$  pc. One-sigma error bars are plotted in all panels, but are often smaller than the plotted data points.

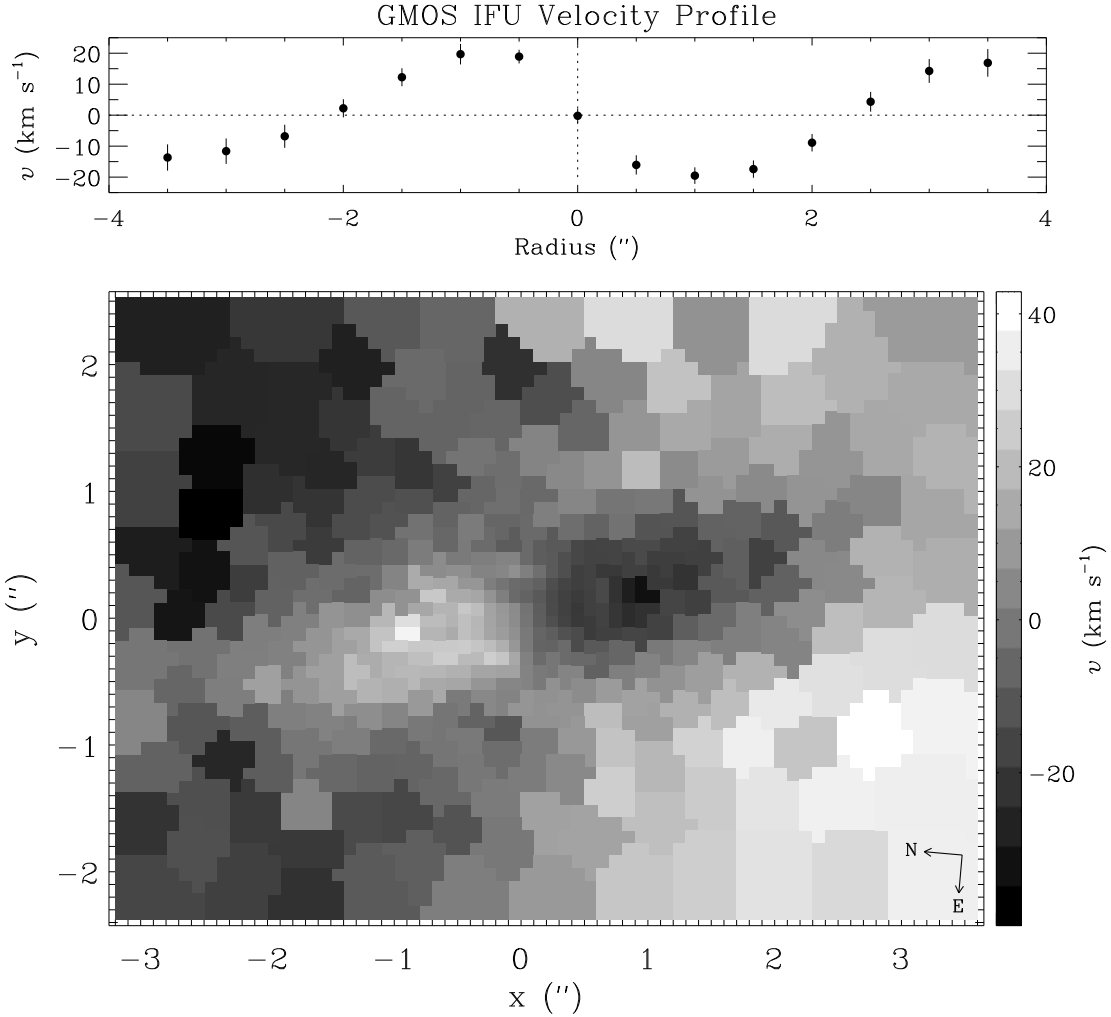


Fig. 4.— (*Bottom*) Stellar velocity ( $v$ ) field for NGC 770 measured with the Gemini GMOS IFU. The optical center of the galaxy corresponds to  $(x, y) = (0, 0)$ . The orientation of the map is shown in the lower right corner. (*Top*) One-dimensional cut through the two-dimensional IFU data averaging over a  $0.75''$  width slit centered and aligned along the axis of counter-rotation. The major-axis profile is symmetric with respect to the galaxy center; the maximum rotation velocity of the counter-rotating region is  $v_{\text{rot}}^{\text{core}} = \pm 21 \text{ km s}^{-1}$ .

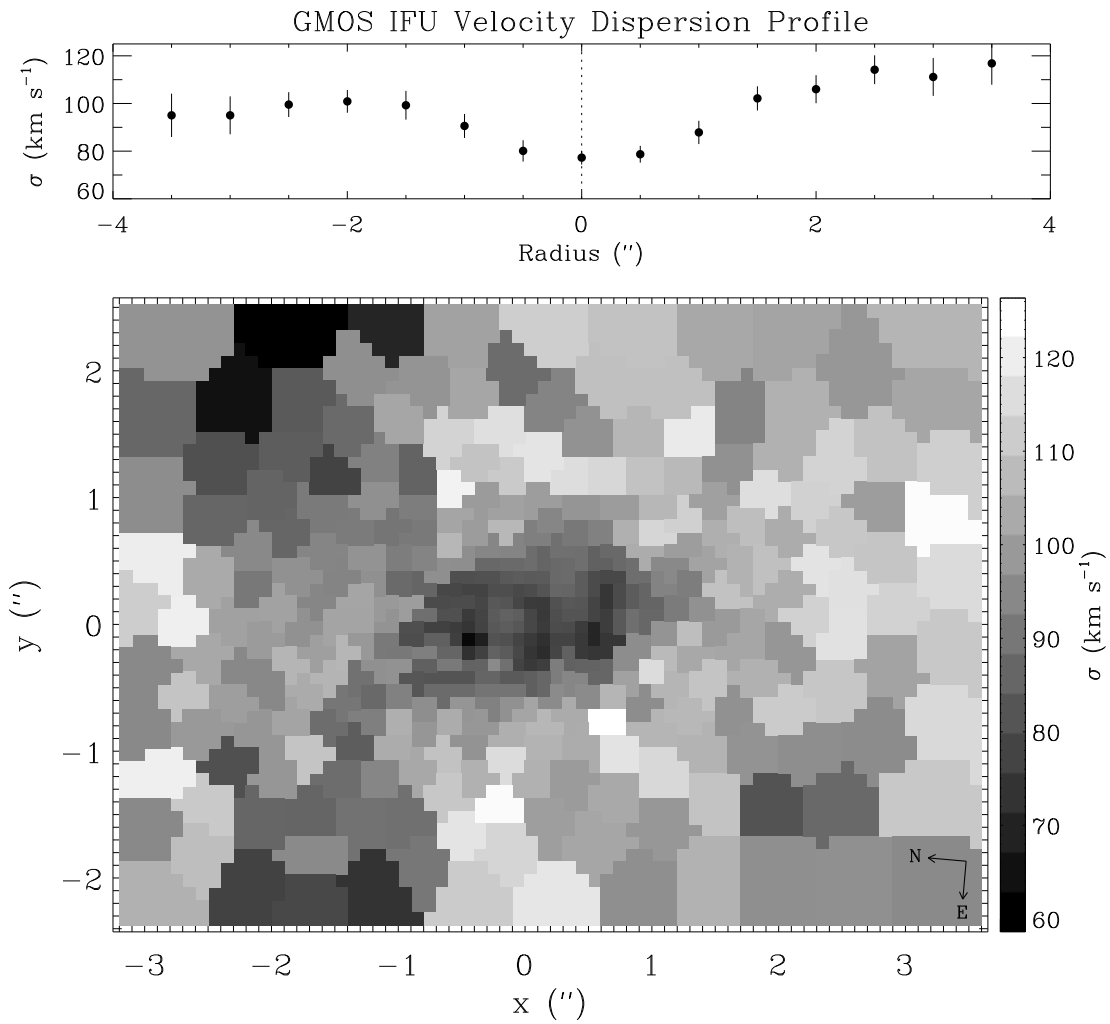


Fig. 5.— Same as Figure 4, except the stellar velocity dispersion ( $\sigma$ ) of NGC 770 measured with the Gemini GMOS IFU is shown.

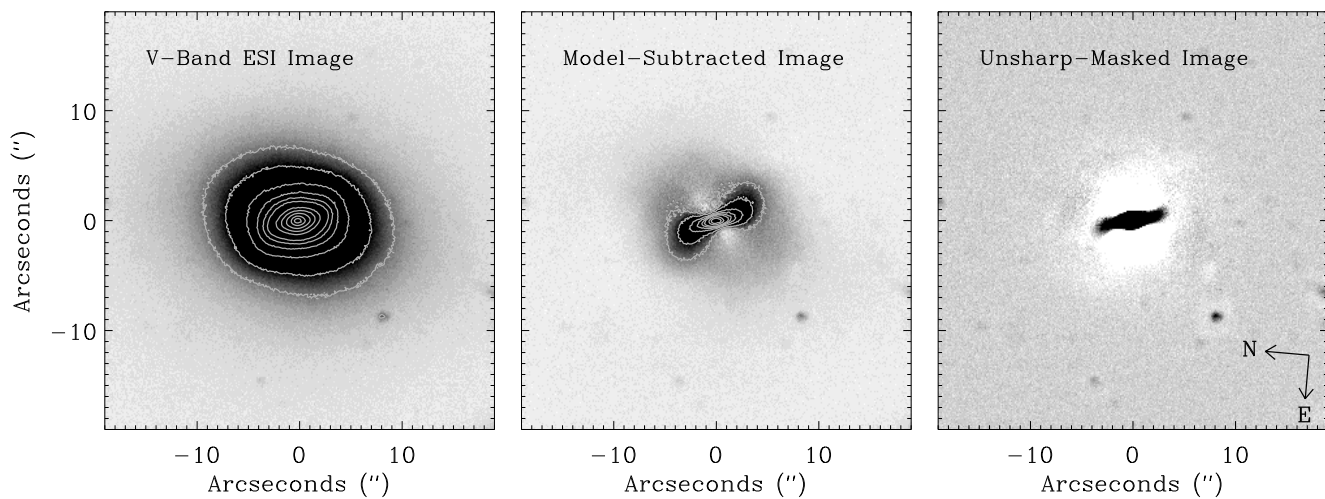


Fig. 6.— (*Left*) Keck/ESI *V*-band image of NGC 770 overlaid with isophotes in the central region. (*Middle*) Residual image created by subtracting a two-dimensional Sersic  $n = 2.3$  profile at a constant position angle and ellipticity from the original image. (*Right*) Unsharp-masked image created by subtracting a smoothed version of the original image from itself (with a 25 pixel = 4'' smoothing length). The contours in the left and middle panels represent the same isophote levels. Each panel covers a 40''  $\times$  40'' region centered on the galaxy and is oriented as indicated in the bottom right corner of the right panel.

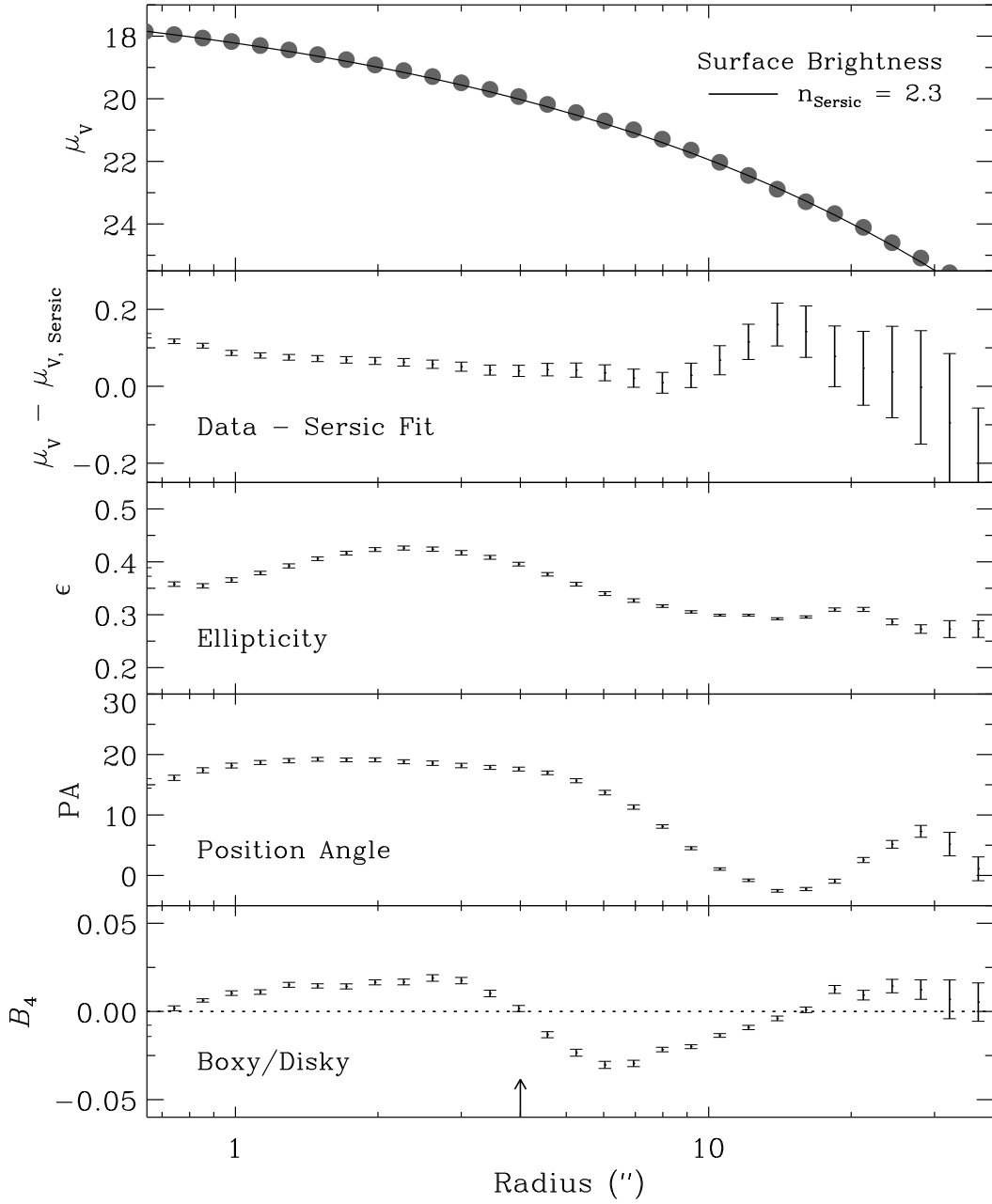


Fig. 7.— Radial profiles for  $V$ -band surface brightness ( $\mu_V$ ), residual surface brightness residuals after subtracting the Sersic fit ( $\mu_V - \mu_{V,fit}$ ), ellipticity ( $\epsilon$ ), position angle (PA) and the boxiness/diskyness parameter ( $B_4$ ) measured from Keck/ESI imaging (*top to bottom*). Positive  $B_4$  values indicate diskly photometric contours, while negative values indicate boxy contours. In the top panel, the best fitting Sersic profile ( $n = 2.3$ ) is plotted over the data. The radial extent of the counter-rotating region as measured in the GMOS velocity map is shown by the arrow at 4" in the bottom panel.



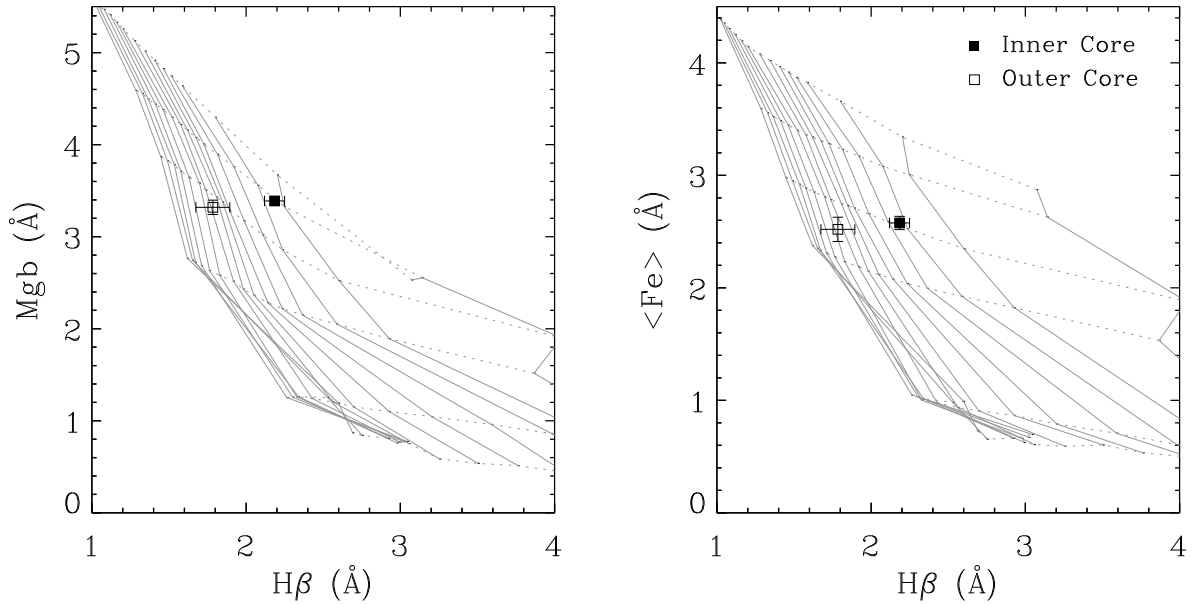


Fig. 8.— Line-strengths Mg b and  $\langle \text{Fe} \rangle$  plotted against  $\text{H}\beta$  (*left and right, respectively*). The solid square is the average line-strength measurement of the inner counter-rotating region ( $r \leq 2''$ ), the open square is the average measurement of the outer core ( $2'' < r < 4''$ ). The solar abundance models of Thomas et al. (2003) are plotted for ages ranging from 1 to 15 Gyr in 1 Gyr intervals (solid grey lines) and  $[\text{Fe}/\text{H}] = -2.25, -1.35, -0.33, 0.0, +0.35,$  and  $+0.67$  dex (dotted lines). In both panels, lines of constant age are steeper than those of constant metallicity.

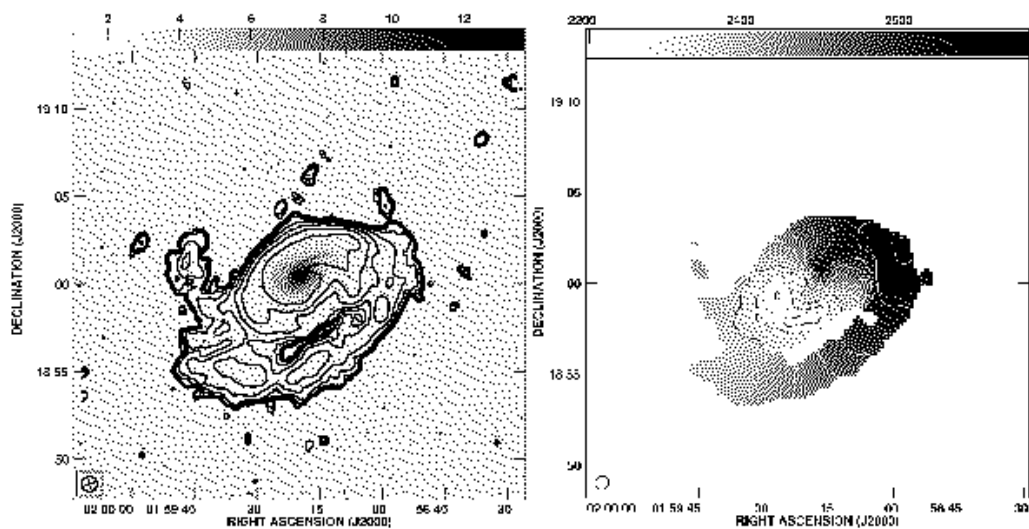


Fig. 9.— (*Left*) Integrated neutral hydrogen HI column density contours over-plotted on a Digitized Palomar Optical Sky Survey image. The contours are between  $0.5\text{--}64 \times 10^{19} \text{ cm}^{-2}$  incremented by factors of two. The beam FWHM of these VLA D-array observations is  $\lesssim 1'$ , indicated in the lower left corner. (*Right*) HI velocity map with iso-velocity contours plotted every  $50 \text{ km s}^{-1}$  over the range  $2250\text{--}2700 \text{ km s}^{-1}$ . These figures were provided by M. Iyer and C. Simpson.